Oceanologia (2017) 59, 460—472

Available online at www.sciencedirect.com

ScienceDirect

journal homepage: www.journals.elsevier.com/oceanologia/

ORIGINAL RESEARCH ARTICLE

Aerosol physical properties in Spitsbergen's fjords: Hornsund and Kongsfjorden during AREX campaigns in 2014 and 2015

Piotr Markuszewski [a,b,*], **Anna Rozwadowska** [a], **Malgorzata Cisek** [a], **Przemysław Makuch** [a], **Tomasz Petelski** [a]

[a] *Institute of Oceanology, Polish Academy of Sciences, Sopot, Poland*
[b] *Centre for Polar Studies National Leading Research Centre, Sosnowiec, Poland*

Received 11 July 2016; accepted 1 March 2017
Available online 25 May 2017

KEYWORDS
Arctic aerosol;
Sea spray;
Black carbon concentration;
Scattering coefficient;
Ångström exponent

Summary We present results of measurements of aerosol physical properties conducted on board of r/v *Oceania* during two cruises to the Spitsbergen region in 2014 (AREX 2014) and 2015 (AREX 2015). Measurements of aerosol size distribution, aerosol scattering coefficient and black carbon concentrations were made in two different Spitsbergen fjords: Hornsund and Kongsfjorden. The aerosol size distribution was measured in the size range from 0.09 μm to 47 μm using two aerosol size distribution spectrometers and a standard condensation particle counter. For the scattering coefficient an integrating nephelometer was used. Black carbon concentration was measured by an aethalometer. Temporal variabilities in physical properties of aerosol observed during the AREX 2014 and AREX 2015 campaigns were much higher than the differences between both fjords. The basic factors influencing aerosol conditions were advection and local generation of marine aerosol. In 2015 an episode of smoke advection was observed in both fjords causing an increase in the mean black carbon concentration from 7—12 ng m^{-3} to about 60 ng m^{-3}, and an aerosol scattering coefficient at 550 nm from 2—4 Mm^{-1} to 12—17 Mm^{-1}. Moreover, under certain conditions statistically significant gradients in aerosol optical properties were observed along the fjord axis reflecting an impact of mountains surrounding the fjords.

* Corresponding author at: Institute of Oceanology, Polish Academy of Sciences, Powstańców Warszawy 55, 81-712 Sopot, Poland. Tel.: +48 (58) 7311901; fax: (+48 58) 551 21 30.
E-mail address: pmarkusz@iopan.gda.pl (P. Markuszewski).
Peer review under the responsibility of Institute of Oceanology of the Polish Academy of Sciences.

ELSEVIER Production and hosting by Elsevier

http://dx.doi.org/10.1016/j.oceano.2017.03.012

1. Introduction

The study of atmospheric aerosols in the marine boundary layer is significant for a variety of climatic issues. Among others, aerosol particles take part in heat, moisture and mass exchange processes. Without understanding the mechanics of aerosol emission and transport it is practically impossible to properly model regional and global weather or climate. Study of aerosol properties in Polar Regions is of particular importance for two reasons, firstly because of very low anthropogenic perturbations there, and secondly because of the strong effect climate changes have on the Arctic. Recent years have seen several measurement campaigns concentrated on aerosol physical properties and transport (Lisok et al., 2016; McFarquhar et al., 2011; Ritter et al., 2016; Tunved et al., 2013). However, only few experiments addressed the differences in aerosol properties between different stations/fjords in the Spitsbergen region.

The study of polar aerosols is always a big challenge, not only because of the isolation of the researched region, but also because of the variety of phenomena occurring in this area. The presence of "Arctic Haze", partially explained by several authors (Quinn et al., 2007; Sharma et al., 2006; Shaw, 1995), and advections of continental air masses containing smoke from forest fires which contributes to enhanced soot concentrations in the Arctic area (Damoah et al., 2004; Stohl et al., 2006) belong to them. Apart from smoke, Asian dust transport has also been observed, mainly in spring (Stone et al., 2010). A comprehensive analysis of atmospheric composition in polar regions was presented by Tomasi et al. (2015). This paper comprises up-to-date knowledge about remote sensing measurements in both Arctic and Antarctic areas.

The challenge of identifying the source regions of Arctic aerosol was taken up by several authors. Large events such as boreal forest fires in Alaska and Canada during the summer of 2004 and its influence on aerosol optical parameters have been studied among others by Stohl et al. (2006). Myhre et al. (2007) and Treffeisen et al. (2007) dealt with another event of pollution and a special meteorological situation in the European Arctic which occurred in 2006. A thorough analysis of the relations between aerosol composition and aerosol optical properties with air masses was presented by Stock et al. (2014). They presented that aerosol optical depth in Ny-Alesund did not depend on the North Atlantic Oscillation.

The comparison of the aerosol optical thickness and the Ångström exponent between northern Norway and Hornsund was presented by Chen et al. (2013). Based on data from AERONET (Aerosol Robotic Network) they found that the four-year annual mean values for the aerosol optical thickness at 500 nm $\tau(500)$ at Andenes and Hornsund were equal to 0.10. Based on analysis of changes in the Ångström exponent (AE) the study concludes that fine-mode particles dominated at both sites. Furthermore, both sites had similar seasonal variations of the aerosol size distribution despite one site being located in the Arctic while the other in a sub-arctic area.

Comprehensive analyses of the optical properties in Hornsund are provided by Rozwadowska et al. (2010) and Rozwadowska and Sobolewski (2010). The authors found that in spring, the changes in AOT values over the station were strongly influenced by long-range advection, mainly from Europe and Asia. The phenomenon of AOT variability in summer was explained by the local direction and speed of advection (1-day trajectories). The impact of distant sources on AOT was strongly modified by cleansing processes en route to Hornsund. However, the highest AOT cases in summer were also associated with long-range transport from Europe, Asia and North America.

Lisok et al. (2016) and Ritter et al. (2016) presented results of measurement of aerosol physical and chemical properties during the iAREA2014 campaign that took place on Svalbard in three stations (Ny—Ålesund, Longyearbyen and Hornsund). The authors' aim was to investigate in situ passive and active remote sensing observations as well as numerical simulations to describe the temporal variability of aerosol single-scattering properties during the spring season on Spitsbergen.

This study presents results of aerosol properties' measurements performed during two Arctic campaigns on board of r/v *Oceania*, AREX (ARctic EXperiment), conducted in 2014 and 2015. The AREX campaign is an annual three-month cruise to the Northern Atlantic, the Nordic Seas and fjords of Spitsbergen. This paper compares aerosol physical properties in Hornsund and Kongsfjorden during the 2014 and 2015 campaigns and relates the differences in these properties to variations in air mass advections and meteorological conditions. The issue of spatial variability of aerosol optical properties in the fjords is also addressed.

2. Area of study

The measurements were carried out in order to investigate variability of aerosol physical properties in two different fjords of Spitsbergen: Hornsund and Kongsfjorden. Hornsund is located in the south of the Spitsbergen area. Kongsfjorden is situated in the northern part of the island (Fig. 1).

The fjords differ from each other with respect to their hydrographic conditions. The Hornsund fjord is cooler than Kongsfjorden because of limited inflow of warm waters from the West Spitsbergen Current (WSC). The mouth of Hornsund is much more often occupied by much lighter and fresher water from of shelf Sorkapp Current which flows from the Barents Sea. The topographical structure of Kongsfjorden, on the other hand, allows for larger injections of warm water from the WSC due to the wide trough of the fjord. Moreover, the shelf current is not influential in this area. A more detailed description of current structures in this area is presented by Walczowski (2013). Differences in locations and hydrographic conditions of the fjords are reflected in differences in local meteorological conditions in the fjords which are discussed with Cisek (personal communication). In both fjords the wind direction is determined mainly by local orography and a horizontal gradient of air temperature, thus in each fjord the dominant wind direction is determined by the axis of the fjord (Svendsen et al., 2002). Moreover, Hornsund has higher wind speeds, humidity and cloud cover than Kongsfjorden. The air temperature, however, is higher in Hornsund only in winter. In summer, the air temperature over Kongsfjorden is higher.

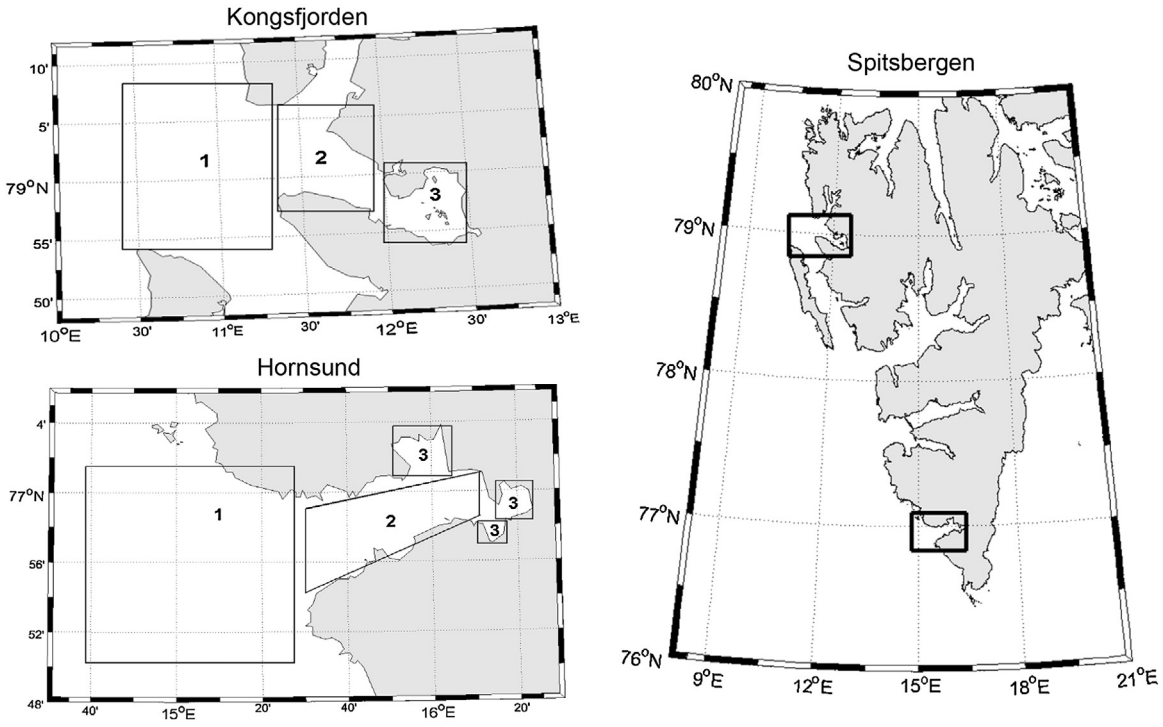

Figure 1 Location of Hornsund and Kongsfjorden and fjords' subregions where the measurements were performed during the AREX campaigns in 2014 and 2015. Numbers represent the fjord subregions: 1 — innermost part of the fjord, 2 — central part, 3 — fjord mouth and the sea outside the fjord.

3. Methods

3.1. Measurements

Measurements of aerosol size distribution, aerosol scattering coefficient and black carbon (BC) concentration were performed during the AREX 2014 and 2015 cruises. In 2014, the measurements in Hornsund were carried out from 25 July (the 206th day of the year) to 1 August (213). In Kongsfjorden, the measurement period lasted from 5 August (217) to 10 August (222). In 2015, the measurements took place in similar periods: from 26 July (207) to 1 August (213) in Hornsund and from 3 August (215) to 9 August (221) in Kongsfjorden.

Aerosol size distribution was assessed by the CSASP-100-HV aerosol spectrometer (manufactured by Particle Measuring System) and a TSI laser aerosol spectrometer 3340 (LAS). The CSASP counts aerosol particles in a diameter range from 0.5 μm to 47 μm in 36 channels. The device was successfully used and described well in several earlier papers (e.g. Petelski et al., 2014; Petelski, 2005; Savelyev et al., 2014; Zieliński, 2004). The LAS counts aerosol particles from diameter size of 0.09 μm up to 7.5 μm in 99 channels. Both instruments use a He—Ne Laser beam. However, thanks to a more sophisticated optical system, the LAS ensures a wider measurement range (Hämeri et al., 2010). In order to compare and check the results from the LAS, a TSI Condensation Particle Counter (CPC) was also used (TSI 3771). The CPC estimates the total aerosol concentration in a diameter range from 0.01 μm to 4.5 μm. However, an analysis of the CPC's measurements is beyond the scope of the present paper.

Equivalent black carbon concentration was measured by a Magee Scientific Company AE-31 aethalometer (e.g. Arnott et al., 2005; Hansen et al., 1984). Equivalent black carbon concentration is the black carbon concentration which—accumulated on a filter — would give the same light attenuation as the actual aerosol accumulated there. However, except for strong mineral dust advections, black carbon is the main aerosol absorber of light. The AE-31 operates in 7 spectral channels: 370, 470, 520, 590, 660, 880 and 950 nm. We used the 520 nm channel for our research. The aerosol accumulation time was set to 1 h and the flow to 65 $cm^3\ s^{-1}$ (3.9 l min^{-1}). Such a long accumulation time was necessary due to the very small aerosol load in the Arctic. The BC concentration is based on measurements of light attenuation by aerosol accumulated on a quartz filter. However, this method is prone to errors due to loading effect. The measurements require correction for this effect when the attenuation of the aerosol accumulated on the filter exceeds 10 (Schmid et al., 2006). During the AREX experiments the filters were changed frequently and the attenuation rarely reached this threshold value. The correction based on Virkkula et al. (2005) was applied in those cases.

Aerosol scattering properties were measured by the TSI nephelometer 3563 (Anderson et al., 1996). The instrument operates on 3 wavelengths: 450, 550 and 700 nm. The measured scattering coefficients were corrected for the effects of non-Lambertian illumination and truncation of scattering in near-forward and near-backward angles using the Anderson and Ogren (1998) method. The scattering coefficients for this research have been averaged to 1 h resolution to match the BC concentration measurements. Detailed descriptions

of the nephelometer and aethalometer are given by Lisok et al. (2016).

During the cruise, all particle counters were situated on a special measurement platform mounted on the fore-mast, 8 m above sea level. The common inlet of the aethalometer and nephelometer was located near the fore-mast, 1 m below the measurement platform.

Meteorological observations from the WMO stations at Ny-Alesund (01007) and Hornsund (01003) were also used in this study for the fjord measurement periods. The meteorological data is available at www.rp5.kz. The standards of WMO meteorological stations are presented by Jarraud (2008).

3.2. Backward trajectories

Six-day backward trajectories (144 h) of the air masses advecting towards the fjords were computed by the NOAA HYSPLIT model (Hybrid Single—Particle Lagrangian Integrated Trajectory Model, Draxler and Hess, 1998) using the GDAS meteorological dataset (Rolph, 2016; Stein et al., 2015). The trajectories were computed for air mass arrival times of 0 and 12 UTC and arrival heights of 500, 1500 and 3000 m. However, only the 500 m trajectories were used in this study.

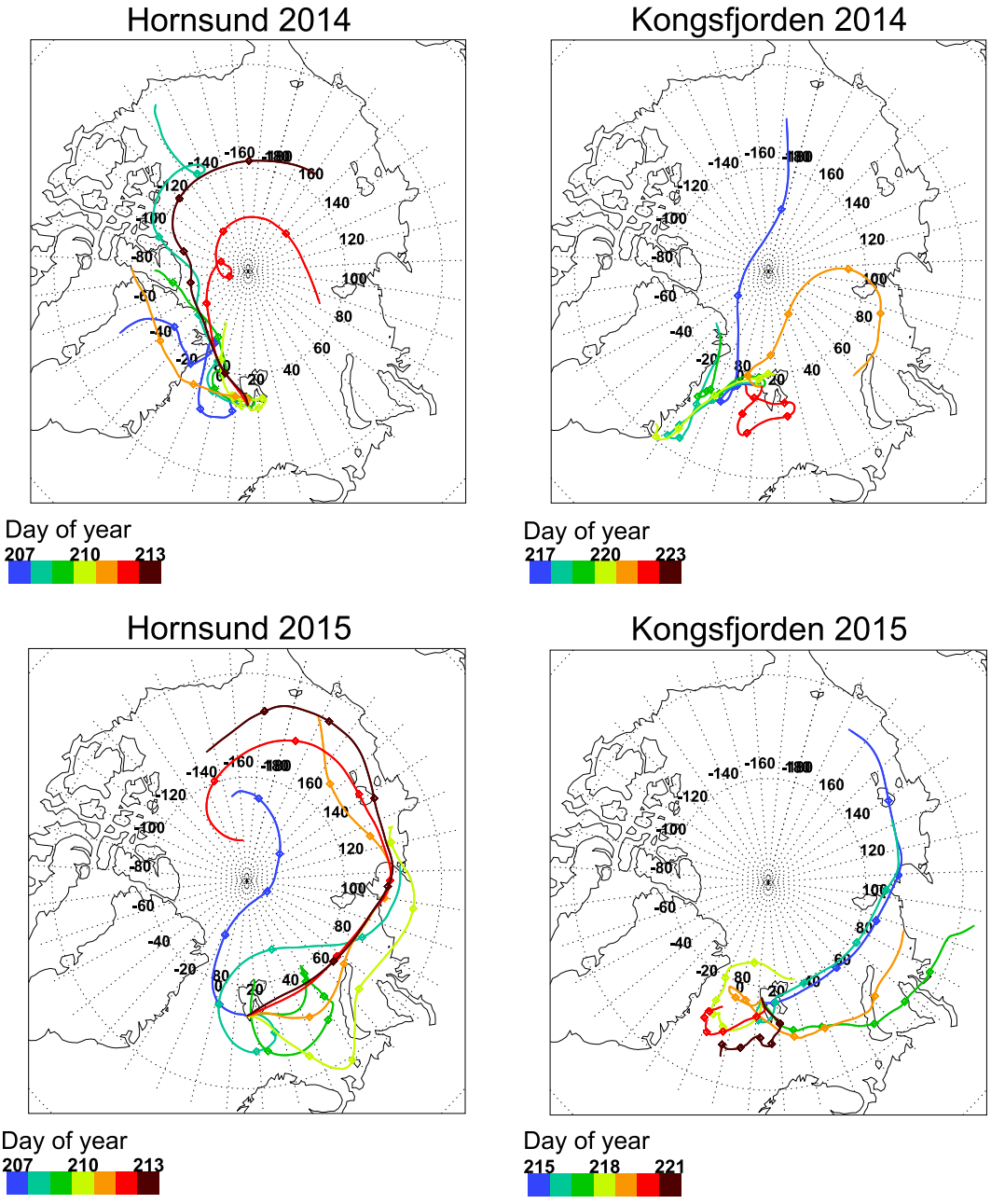

Figure 2 Back-trajectories of air masses arriving at 500 m above Hornsund (left) and Kongsfjorden (right) during aerosol measurements in the fjords. The trajectories were computed for 12 UTC on a day indicated by the trajectory colour. (For interpretation of the references to color in this figure legend, the reader is referred to the web version of this article.)

3.3. Definitions of physical quantities used in this work

The basic aerosol size distribution parameters used in this paper are: zero moment M_0 (mean aerosol concentration), first moment M_1, mean particle diameter $\overline{D_p}$ and effective radius r_e. These parameters are defined as follows:

$$M_0 = \sum_{i=1}^{k} N_i, \tag{1}$$

$$M_1 = \sum_{i=1}^{k} N_i D_{p_i}, \tag{2}$$

$$\overline{D_p} = M_1 M_0^{-1}, \tag{3}$$

$$r_e = \left(\sum_{i}^{k} r_i^3 N_i\right)\left(\sum_{i}^{k} r_i^2 N_i\right)^{-1}, \tag{4}$$

where N_i is the aerosol concentration in the interval (instrument channel) i with the diameter D_{pi} and the $r_i = D_{pi}$*0.5 which is the particle radius.

In the paper, aerosol scattering properties are characterized by scattering coefficient at light wavelength of 550 nm, b, and Ångström exponent, AE, of the scattering coefficient spectrum $b(\lambda)$ representing the slope of the scattering coefficient spectrum in a log-log scale:

$$b(\lambda) = b(\lambda_0)e^{-AE}, \tag{5}$$

where λ_0 is a selected wavelength, usually λ_0 = 1 μm resolution. In this work, AE was estimated using linear fitting in log-log scale for the spectral range of 450–700 nm. In this paper, we discuss hourly means of b and AE.

4. Results and discussion

4.1. Air-mass advection and meteorological conditions during measurement period

The campaign periods of 2014 and 2015 differ distinctively in both advection directions and meteorological conditions. In 2014, air masses from northern Greenland, the Canadian Arctic Islands and the Arctic Ocean dominated in the atmospheric boundary layer (trajectory arrival height of 500 m over the station) over both Hornsund and Kongsfjorden (Fig. 2) with 9 August 2014 (221) as an exception when the

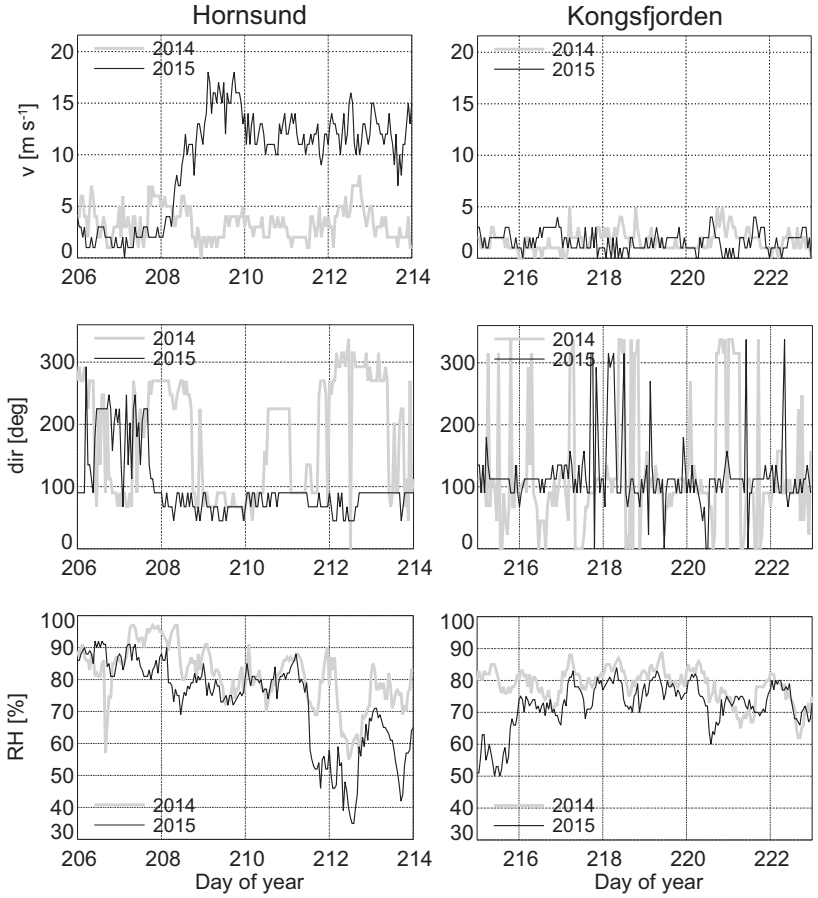

Figure 3 Meteorological conditions at the Hornsund (Hornsund fjord) and the Ny Ålesund (Kongsfjorden) WMO stations: wind speed (v), wind direction (dir) and relative humidity (RH during aerosol measurements in the fjords (AREX 2014 and 2015). Wind direction angles are determined clockwise starting from the North, i.e. 0° is N, 90°E, 180°S and 270°W.

air-mass back-trajectories led from the vicinity of Nova Zemlya over the Arctic Ocean to Kongsfjorden.

In 2014 meteorological conditions in both fjords did not change significantly during the experiment (Fig. 3). During the campaign, wind speeds, *v*, in both fjords were typically < 5 m s^{-1} with values slightly higher in Hornsund than in Kongsfjorden. In Hornsund *v* exceeded 5 m s^{-1} during the analyzed time period. Wind directions (at 10 m) close to the main axis of the fjords dominated regardless of the direction of winds in the free troposphere. Hornsund stretches from West to East, while Kongsfjorden lies along a NW-SE direction. This was reflected in dominant wind directions: E and W in Hornsund and from E, ESE and N in Kongsfjorden. Relative humidity (RH) fluctuated around 80% with a negative trend. The RH fluctuations were stronger in Hornsund than in Kongsfjorden. In Hornsund RH $>$ 90% was observed on 26 and 27 July 2014 (207 and 208) and RH $<$ 70% on 31 July (212); in Kongsfjorden on 9 and 10 August 2014 (221 and 222).

In 2015 advection patterns were more variable (Fig. 2). From 25 to 27 July (206—208) the air masses over Hornsund came from the Arctic Ocean with the exception of the short period on 26 July (207, 0 UTC) when the trajectory originated over the Siberian coast, near the Taymyr and Yamal Peninsulas. Starting on 27 July (208) the advection pattern began to gradually change. On 27 (208, 12 UTC) and 28 July (209, 0 UTC) the trajectories lead from the vicinity of the Taymyr Peninsula, went around Spitsbergen from the north side and reached Hornsund from the south-east. From 28 July (209, 12 UTC) to 29 July (210, 0 UTC) Hornsund was under inflow from the Barents Sea. After that, the air masses from the Siberian coast affected the Spitsbergen area. Six-day trajectories originated near the Taymyr Peninsula, passed Nova Zemlya and reached Hornsund from the south. Starting from 30 July (211) air masses from the Arctic Ocean near the Chukotka Peninsula and Alaska advected to Hornsund, crossing the Taymyr Peninsula. The air mass movement was fast and the air reached Hornsund from the east. This circulation pattern was also observed for Kongsfjorden and continued up to 4 August (216, 0 UTC) at which time the trajectories gradually shortened, indicating slower air-mass movement, and reached Kongsfjorden from the southwest (4 August, 216) and south (5 August, 217). On 6 August (218), Kongsfjorden was influenced by local air masses from the Greenland Sea. On 7 August (219), the air masses arriving over Kongsfjorden again originated over the Taymyr Peninsula. Loops on the trajectories indicated that the advection was associated with low pressure systems. Starting from 8 August 220) to the end of the measuring period, the air masses in Kongsfjorden advected from the Greenland Sea.

Meteorological conditions in Hornsund in 2015 were more dynamic than in 2014 (Fig. 3). During the measuring cam-

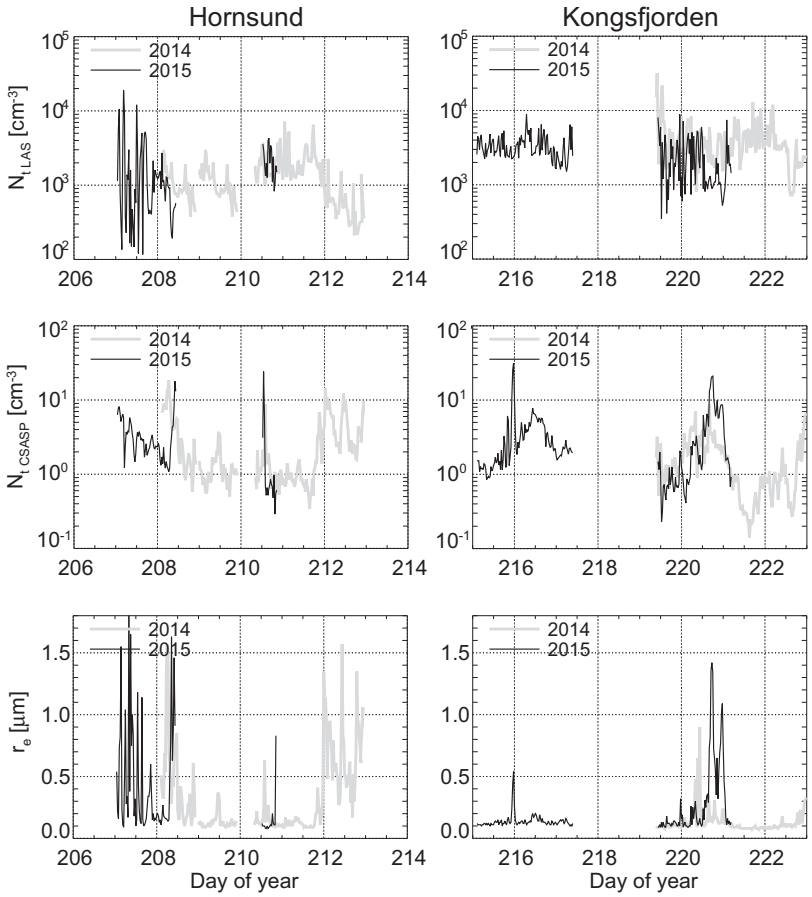

Figure 4 Time series of total aerosol concentration from the particle counters used during the measurements in Hornsund and Kongsfjorden in 2014 and 2015: LAS ($N_{t\,LAS}$, particle radius range: 0.09—7.5 μm) and CSASP ($N_{t\,CSASP}$, particle radius range 0.5—47 μm), and aerosol effective radius (r_e) computed on the basis of the particle counters' measurements (Eq. (4)).

paign, winds from the East (Hornsund) and ESE (Kongsfjorden) dominated. From 28 July to 1 August (209–213) strong eastern winds occurred (with their speed greater than 10 m s^{-1}) in Hornsund. However, wind speed was <5 m s^{-1} throughout the whole Kongsfjorden's part of the campaign. The advection from Siberia was also associated with small RH values. From 30 July to 1 August (211–213) RH < 60% (Hornsund) was observed. In Kongsfjorden RH < 60% was found on 3 August (216).

4.2. Aerosol size distribution observations

Table 1 presents total aerosol concentration characteristic for each particle counter, such as mean aerosol concentration M_0, mean standard deviation, minimum and maximum values for each fjord and the whole period of measurements. Additionally, basic aerosol size distribution parameters are presented such as zero moment M_0 (mean aerosol concentration, Eq. (1)), first moment M_1 (Eq. (2)) and the mean particle diameter (Eq. (3)). Fig. 4 presents time series of total aerosol particle concentrations from all three particle counters.

During the campaign in 2015 for the CSASP size range of measurements higher total aerosol particle concentrations were observed in both fjords. For Hornsund, the mean concentration values were 2.9 cm^{-3} in 2014 and 7.4 cm^{-3} in 2015. A similar situation was observed in Kongsfjorden but with smaller differences. Furthermore, in Hornsund the medium particle diameter was higher than in 2015 (where values changed from 3.07 μm in 2014 up to 3.50 μm in 2015). In Kongsfjorden the situation was opposite to Hornsund, smaller particles dominated in 2014 ($\overline{D_p}$ varied from 3.55 μm in 2014 up to 2.82 μm in 2015). The case was different for smaller particles measured using the LAS. M_0 in 2015 were lower than in 2014 for both fjords. The mean diameters of particles in Kongsfjorden were larger by approximately 0.7 μm.

4.3. Aerosol optical properties observations

In 2014 during both parts of the cruise very low black carbon concentrations in the atmosphere was recorded, with mean BC concentrations lower than 8 ng m^{-3}, and low scattering coefficient b(550 nm) (≥2–3 Mm^{-1}). Low values of these parameters were associated with dominant western advections (Fig. 2). Fig. 5 shows the time series of these properties. The measurements reveal that local aerosol generation from the fjord surface or marine aerosol advection from the sea in the vicinity of Spitsbergen have a significant impact on aerosol optical properties for both fjord regions during the 2014 campaign. This is indicated by a considerable correlation between AE and b(550 nm) (R = −0.58 and −0.51 in Hornsund and Kongsfjorden respectively) and between AE and v (R = −0.42 and −0.54). A high positive correlation coefficient between the scattering coefficient and the effective radius of aerosol particles (R = 0.55 and 0.84 in Hornsund and Kongsfjord respectively) also suggest that an increase in aerosol scattering is caused by large particles. All the correlation coefficients showed in this paper are statistically significant at the level of 0.001. The measurements performed during the campaigns did not allow us to observe any impact of RH on aerosol optical properties. Even though

Table 1 Basic characteristics of mean aerosol size distributions from measurements with CSASP (particle radius range of 0.5–47 μm), LAS (0.09–7.5 μm) and CPC (0.01–4.5 μm) in Hornsund (H) and Kongsfjorden (K) during the 2014 and 2015 AREX cruises. M_0 is the zero moment (mean total aerosol concentration), M_1 is the first moment and $\overline{D_p}$ is the mean particle diameter defined as in Eqs. (1)–(3). σ is the standard deviation and Min, Max are respectively the minimum and maximum values of the total aerosol concentrations.

	CSASP						LAS						CPC			
	M_0 [cm^{-3}]	M_1 [cm^{-3} μm^{-1}]	$\overline{D_p}$ [μm]	σ [cm^{-3} μm^{-1}]	Min [cm^{-3}]	Max [cm^{-3}]	M_0 [cm^{-3}]	M_1 [cm^{-3} μm^{-1}]	$\overline{D_p}$ [μm]	σ [cm^{-3} μm^{-1}]	Min [cm^{-3}]	Max [cm^{-3}]	M_0 [cm^{-3}]	σ [cm^{-3} μm^{-1}]	Min [cm^{-3}]	Max [cm^{-3}]
H 2014	2.9E+00	1.0E+01	3.1E+00	2.1E+00	7.3E−01	1.0E+01	2.0E+03	2.4E+02	1.3E−01	1.1E+03	7.5E+02	4.9E+03	8.9E+02	2.2E+03	3.6E+02	5.4E+04
H 2015	7.4E+00	2.7E+01	3.5E+00	4.4E+00	3.0E+00	2.1E+01	1.4E+03	1.6E+02	1.3E−01	1.3E+03	2.8E+02	6.5E+03	1.9E+03	6.7E+03	6.0E+01	9.1E+04
K 2014	1.7E+00	5.8E+00	3.6E+00	1.2E+00	4.5E−01	9.1E+02	4.4E+03	4.3E+02	1.4E−01	3.3E+03	1.2E+03	1.6E+04	1.1E+03	1.1E+03	1.4E+02	6.3E+04
K 2015	3.2E+00	9.6E+00	2.8E+00	3.0E+00	9.8E−01	1.6E+01	3.0E+03	4.1E+02	1.7E−01	1.6E+03	1.2E+03	7.7E+03	1.9E+07	3.2E+03	2.7E+02	5.8E+04

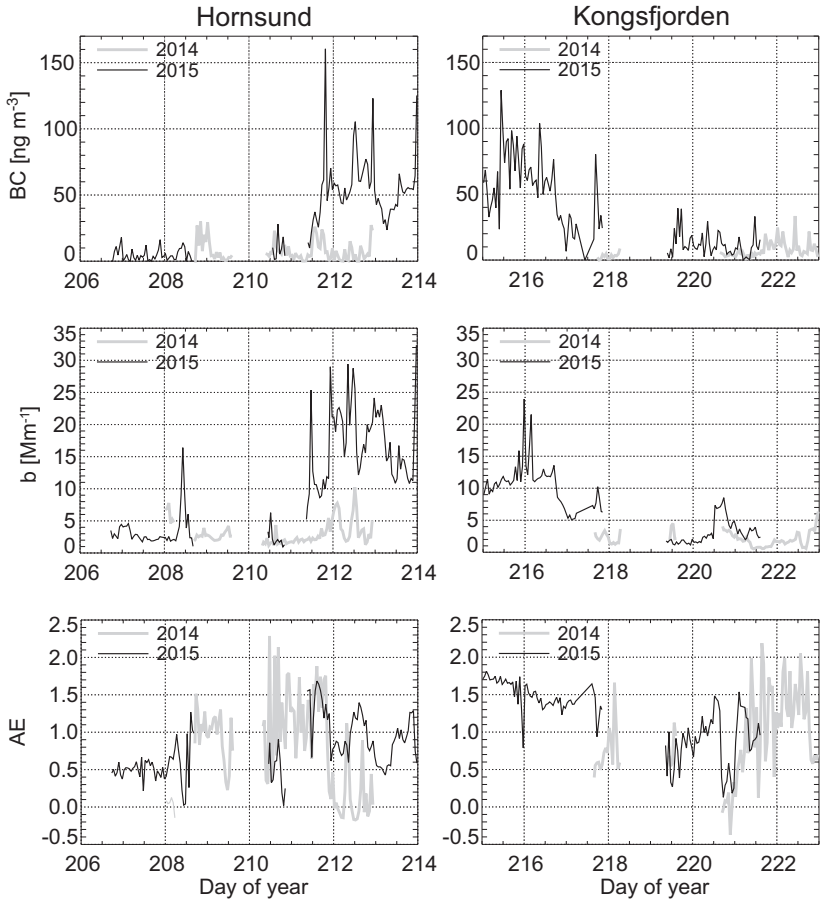

Figure 5 Time series of aerosol optical properties measured during the campaign in Hornsund and Kongsfjorden in 2014 and 2015: black carbon concentration (BC), scattering coefficient (b) and the dimensionless Ångström exponent (AE).

ambient RH was high enough to affect particle size, and thus the scattering coefficient, RH in the nephelometer chamber was below 57%, so the impact of RH on measured b(550 nm) can be deemed negligible or small during the fjord periods of both AREX campaigns.

In 2015, variability in aerosol optical properties was mainly caused by smoke advection. Distinct periods of elevated BC concentrations and scattering coefficient were observed in both fjords, which caused increased values of the mean aerosol scattering coefficient and BC concentrations. Correlation between b and BC was high in both Hornsund (R = 0.76) and Kongsfjorden (R = 0.79). It must be noted, however, that the simultaneous occurrence of large BC values and high wind speeds in Hornsund strengthened this correlation for Hornsund. Elevated BC and b(550 nm) values occurred during fast advection of air masses from the Siberian coast and the Arctic Ocean near the Chukotka Peninsula and Alaska. Smoke brought by this advection could come from fires occurring at that time in Canada (near the Great Slave Lake) and in Alaska (https://firms.modaps.eosdis.nasa.gov/firemap/). They could also be remnants of smoke from strong forest fires in Canada from the beginning of July, still present in the Arctic atmosphere. Moreover, during the fjord stage of the AREX 2015 campaign, fires were also reported in Siberia (Yamalo-Nenetskiy Avtonomyy Okrug — northern part of the West Siberian Plain, and on the Chukotka Peninsula). The elevated BC concentration and scattering coefficient lasted from noon on 30 July to 5 p.m. on 4 August (211—216). Further in this paper, this period is referred to as “advection period” or “smoke advection period”. The periods with small values of BC and b are referred to as 'background'. When the ship was in Hornsund in 2015, the background period lasted from 25 July to 29 July (206—210). It was also observed from 8 to 9 August 2015 (220—221) during the ship's stay in Kongsfjorden. Measurements from 2014 were also treated as “background” measurements.

During the smoke advection period in 2015 the respective mean values (±standard deviation) of BC, b(550 nm) and AE were 56.6 ± 24.2 ng m^{-3}, 17.08 ± 5.70 Mm^{-1} and 0.96 ± 0.32 in Hornsund, and 67.5 ± 21.2 ng m^{-3}, 12.16 ± 2.86 Mm^{-1} and 1.55 ± 0.19 in Kongsfjorden. In spite of a lower BC concentration in Hornsund than in Kongsfjorden, the scattering coefficient was higher in Hornsund. This was due to high winds in Hornsund during the smoke advection period (up to 15 m s^{-1}). When the ship moved to Kongsfjorden the wind speed decreased drastically ($v < 4$ m s^{-1}). A considerable contribution of sea spray aerosol in Hornsund are indicated by high correlation coefficients: R = 0.47 for b versus v, −0.61 for AE versus b. Outside the advection period (background period), BC, b and AE values in both fjords were similar to each other and comparable with values measured in 2014 (Table 2).

Table 2 Means and standard deviations of aerosol scattering coefficient (b), Ångström exponent (AE) and black carbon concentration (BC) measured in Hornsund (H) and Kongsfjorden (K) during the 2014 and 2015 AREX cruises. The index "s" stands for "smoke advection" and "b" means "background" periods. Both periods are defined in Section 4.3.

	Nephelometer		AE-31
	b(550 nm) [Mm^{-1}]	AE	BC [ng m^{-3}]
H 2014	3.10 ± 1.83	0.78 ± 0.64	7.7 ± 7.8
H 2015	10.20 ± 8.26	0.77 ± 0.37	31.9 ± 31.4
K 2014	2.12 ± 1.16	0.92 ± 0.57	6.9 ± 6.0
K 2015	7.02 ± 4.67	1.20 ± 0.42	29.1 ± 23.2
H_s 2015	17.08 ± 5.70	0.96 ± 0.32	56.6 ± 24.2
K_s 2015	12.16 ± 2.86	1.55 ± 0.19	67.5 ± 21.2
H_b 2015	3.29 ± 2.51	0.53 ± 0.24	4.8 ± 4.6
K_b 2015	3.73 ± 1.97	0.92 ± 0.38	10.5 ± 7.3

4.4. Long-range advection and local aerosol generation — their impact on aerosol optical properties

A typical approach in the study of aerosols over oceans is to relate aerosol properties, e.g. b or AE, to wind speed being a proxy of local aerosol generation (e.g. O'Dowd et al., 2010; Smirnov et al., 2003; Vaishya et al., 2012). However, the measurements performed in the Kongsfjorden and Hornsund fjords show that the effects of advections should not be neglected in such relationships even in remote Arctic sites. Fig. 6 compares the impacts of marine aerosol generation, represented by wind speed, and smoke advection on b and AE in Hornsund and Kongsfjorden during the AREX 2015 campaign. In Fig. 6, "H" and "K" stand for Hornsund and Kongsfjorden respectively, and indices "s" and "b" denote smoke advection and background periods. Separate plots are given for measurements from the interior of the respective fjord (regions 2 and 3 defined in Fig. 1) and the fjord mouth and the adjacent ocean area (region 1). The low-wind ($v < 5$ m s^{-1}) background values of b for the fjords were the same inside Hornsund and Kongsfjorden (subregions 2 and 3; 3 ± 1 Mm^{-1}). In Kongsfjorden the smoke advection caused an increase in scattering coefficient by about 10 Mm^{-1} with respect to the non-advection period (an increase to 12.8 ± 3.0 Mm^{-1}). This difference is statistically significant at the level of 0.05. Given a nearly constant b with v within the range of 0–10 m s^{-1}, we may assume a similar increase in b in Hornsund due to smoke advection alone during that period. Further increase in b, up to 30 Mm^{-1}, was due to marine aerosol generation and was observed when wind speeds exceeded 10 m s^{-1}. Smoke advection also influenced AE, causing its statistically significant increase from AE = 1.05 ± 0.22 to AE = 1.49 ± 0.19 in Kongsfjorden (subregions 2 and

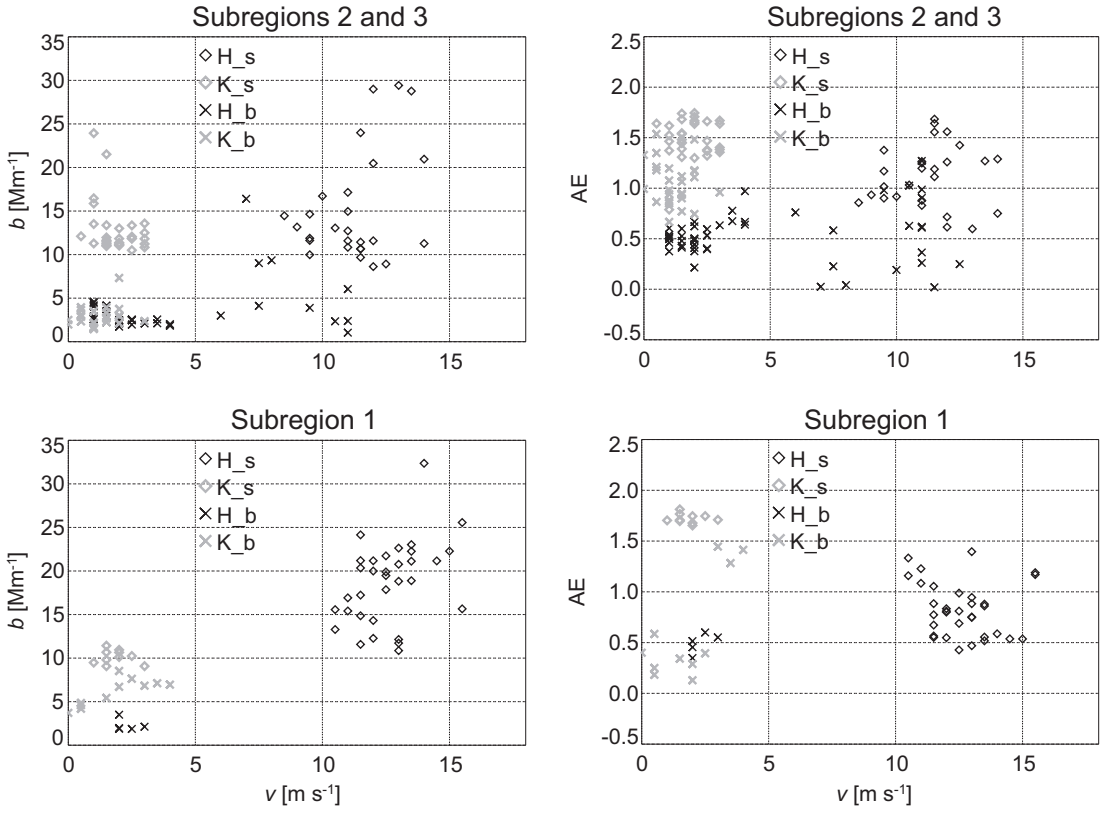

Figure 6 Dependency of aerosol scattering coefficient b(550 nm) and Ångström exponent (AE) on marine aerosol generation, represented by wind speed, and smoke advection in 2015. H and K denote respective measurements from Hornsund and Kongsfjorden, "s" stands for "smoke advection" and "b" means "background", i.e. non-smoke advection period. Fjord regions are defined in Fig. 1.

3; $v < 5$ m s^{-1}). A similar value of an increase in the Angstrom coefficient is also expected in Hornsund (from 0.53 ± 0.14 to about 1.00). Given the limited data the impact of wind speeds on AE cannot be precisely determined in the fjords. However, based on Fig. 6, AE seems to be less sensitive to local wind generation than to smoke advection.

Measurements performed in the fjords in 2015 reveal that long-range advection can considerably affect optical properties of aerosols in the Arctic. Further, negligence of its impact may lead to false conclusions. An example is shown in Fig. 6. A negligence of advection impact would result, for example, in a false, positive correlation between AE and v for Hornsund. This is because the smoke advection occurred simultaneously with strong winds in Hornsund and the smoke and marine aerosol had the opposite impact on AE. While the presence of fine smoke particles increased AE by about 0.5—1, the coarse mode sea spray aerosols reduced it. When the impact of the smoke aerosol on AE dominates, we obtain a positive correlation coefficient between v and AE.

4.5. Spatial variability of aerosol properties in a fjord

The last issue addressed in this paper is the dependence of aerosol optical properties on the location of the sampling site in a fjord. For this purpose, three subregions were selected in both Hornsund and Kongsfjorden (Fig. 1): the mouth of a given fjord and the adjacent ocean area (subregion 1), the central part of the fjord (subregion 2) and the innermost part of the fjord including lateral fjords (subregion 3). Measurements from subregion 3 are expected to be most affected by the land surrounding a given fjord, while the measurements from region 1 should be closest to oceanic conditions. Measurements from region 2 can be treated as representative of a given fjord. Furthermore, for each fjord we selected cases of meteorological conditions for which measurements were performed in all the fjord subregions. For Hornsund, the following cases were selected: the smoke advection period with winds from the fjord interior (N-E-S wind directions; 350—170°) and v within the range of 11—13 m s^{-1} (Hornsund, case 1) as well

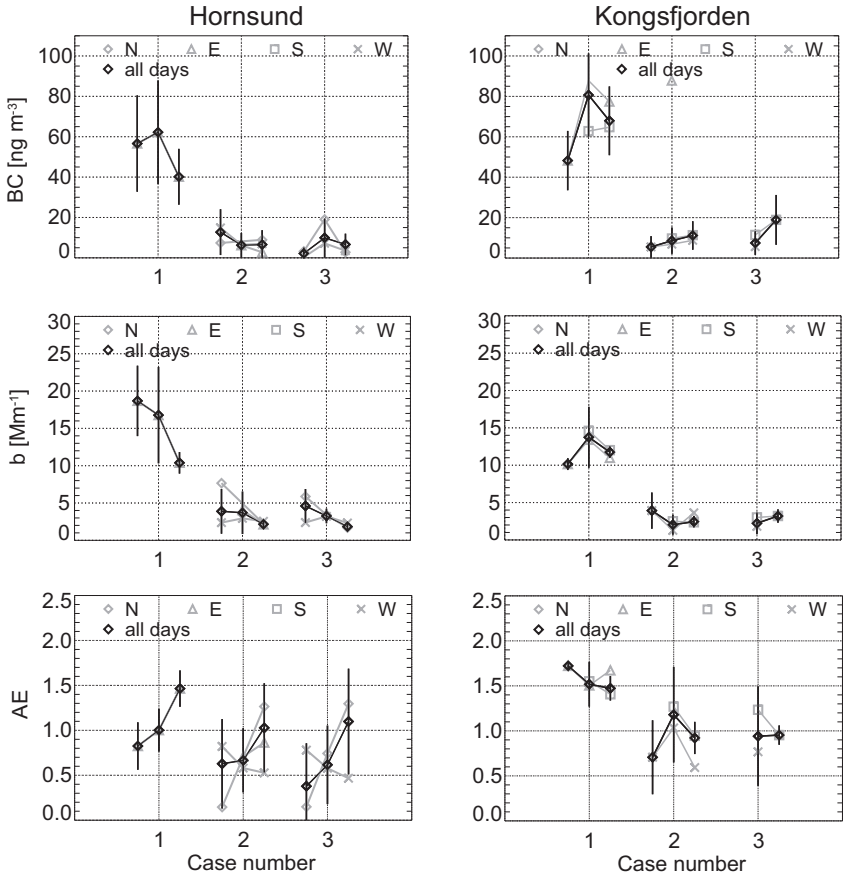

Figure 7 Dependency of black carbon concentration (BC), scattering coefficient (b) and the dimensionless Ångström exponent (AE) on the location of measurement sites in Hornsund and Kongsfjorden. The location is expressed as a respective fjord subregion defined in Fig. 1. Numbers below the plot for BC (Hornsund, case 1) are subregion numbers and show the order of subregions in all the plots. Cases are defined as follows: Hornsund 1 — smoke advection period, wind direction of 350°—170°, v = 11—13 m s^{-1}, Hornsund 2 — background period, wind direction of 350°—170°, $v < 4$ m s^{-1}, Hornsund 3 — background period, wind direction of 170°—350°, $v < 4$ m s^{-1}, Kongsfjorden 1 — smoke advection period, wind direction of 5°—180°, $v < 4$ m s^{-1}, Kongsfjorden 2 — background period, wind direction of 20°—200°, $v < 4$ m s^{-1}, Kongsfjorden 3 — background period, wind direction of 20°—200°, $v < 4$ m s^{-1}. Black symbols and lines show the means and standard deviations for all the measurements within a given case. Grey symbols represent means for selected directions of air mass arrival at a given fjord (E — east, W — west, S — south, N — north).

as winds from the fjord interior (N-E-S; Hornsund, case 2) and the ocean (S-W-N 170–350°; Hornsund, case 3) with $v < 4$ m s^{-1} during the background periods in 2015 and in 2014. Wind speeds less than 4 m s^{-1} ensure a lack of local aerosol generation in the fjord. The cases selected for Kongsfjorden are as follows: smoke advection with winds from the fjord interior (NNE-SSW, 20–220°) with $v < 4$ m s^{-1} (Kongsfjorden, case 1) as well as background periods (2014 and 2015) with wind speeds < 4 m s^{-1} and wind directions from the fjord (Kongsfjorden, case 2) and ocean (Kongsfjorden, case 3). Additionally, within each case the data was divided into subcases with respect to the direction of air mass advection to a given fjord, just before the air mass reached the fjord. The mean values of BC, *b* and AE for each case and each sector are shown in Fig. 7. Locations of points for each case in the plot are in agreement with the geographical position of the respective fjord subregions, i.e. from east (subsection 1, leftmost point) to west (subsection 3, rightmost point).

For all the Hornsund cases an increase in AE is observed in the inner part of the fjord with respect to the fjord mouth while BC and *b* usually decrease (cases 1 and 2 for BC, and 1 and 3 for *b*). The differences between the respective values for subregion 1 and 3 are statistically significant at the level of 0.05. In Kongsfjorden, BC increases moving from the fjord mouth to its innermost part (all cases) while for *b* and AE the changes are less pronounced. Moreover, in Hornsund the main differences between the optical properties of aerosols are found for the central and inner parts of the fjord; in Kongsfjorden the largest differences were typically observed between subregion 1 (the fjord mouth and the adjacent ocean) and the central part of the fjord (subregion 2).

In the case of the fast advection along a fjord axis (Hornsund case 1, easterly winds; 30 July, 211 day of the year, to 1 August, 213) relatively strong gradients in aerosol optical properties were observed. The scattering coefficient decreased from the outside of the fjord to the innermost part of the fjord (from 19 to 10 Mm^{-1}), while AE increased (from 0.83 to 1.46) indicating the smaller contribution of coarse mode marine aerosols inside the fjord at the time. The differences in *b* and AE between subregions 1 and 3 are statistically significant at the level of 0.05. In Hornsund similar tendencies were also observed in the cases of weak winds ($v < 4$ m s^{-1}) regardless of their direction (cases 2 and 3), especially in the case of advection from the north (grey diamonds in Fig. 7). The separation of data with respect to advection direction indicates that gradients of aerosol properties in Hornsund largely depend on the direction of large scale wind fields in the vicinity of the fjord with respect to the axis of the fjord (compare subcases of case 2 and 3 for Hornsund). It must be remembered, however, that the measurement in different parts of the fjords and in different fjords we not performed simultaneously; they are displaced in time with respect to each other. Moreover, the number of measurements is very limited and the time period of the measurements is very short. Therefore, the results presented in this section must be treated as preliminary. The problem requires further study.

5. Conclusions

The temporal variability in physical properties of aerosols observed during the AREX 2014 and AREX 2015 campaigns was much higher than the differences between the Hornsund and Kongsfjorden fjords. Outside the smoke advection period in 2015, BC, *b* and AE values in both fjords were similar to each other. The mean values of the aerosol characteristics analyzed in this study are given in Tables 1 and 2 for each of the fjord and different periods.

The important factor influencing aerosol conditions during the AREX 2014 and 2015 campaigns was the generation of marine aerosols. This conclusion is supported with high correlations between the Angstrom exponent AE and scattering coefficient *b*, and between AE and wind speed.

In 2015, an episode of smoke advection was observed in both fjords causing an increase in BC concentrations from 7–12 ng m^{-3} to about 60 ng m^{-3}, and scattering coefficient from 2–4 Mm^{-1} to 12–17 Mm^{-1}. Its significantly increased BC concentration, *b* and AE values in both fjords (compare Table 2).

Under certain conditions statistically significant gradients in aerosol optical properties were observed along the fjord axis reflecting an impact of mountains surrounding the fjord on aerosol distribution in a fjord. In Hornsund, a statistically significant increase in the Ångström exponent and reduction in the scattering coefficient were found (moving from the fjord mouth and adjacent ocean to the fjord innermost regions) for fast easterly advection of biomass burning aerosol (wind speed in the fiord of 11–13 m s^{-1}) and northerly advection (wind speed in a fjord of <4 m s^{-1}) (compare Fig. 7).

In Hornsund the main differences between the optical properties of aerosols were found for the central and inner parts of the fjord; in Kongsfjorden the largest differences were usually observed between subregion 1 (the fjord mouth and the adjacent ocean) and the central part of the fjord (subregion 2).

In this study we show complexity of phenomena influencing spatial variability of aerosol properties such as orography or meteorological conditions. However, these phenomena need further comprehensive studies.

Acknowledgments

This work was supported through the National Science Centre grant id. number: 2015/17/N/ST10/02396, by funds from the GAME "Growing of the Arctic Marine Ecosystem" project funded by the National Science Centre grant DEC-2012/04/A/NZ8/00661, and the Polish-Norwegian Research Programme operated by the National Centre for Research and Development under the Norwegian Financial Mechanism 2009–2014 as part of Project Contract No Pol-Nor/196911/38/2013.

References

Anderson, T.L., Covert, D.S., Marshall, S.F., Laucks, M.L., Charlson, R.J., Waggoner, A.P., Ogren, J.A., Caldow, R., Holm, R.L., Quant, F.R., Sem, G.J., Wiedensohler, A., Ahlquist, N.A., Bates, T.S., 1996. Performance characteristics of a high-sensitivity, three-wavelength, total scatter/backscatter nephelometer. J. Atmos. Ocean. Technol. 13, 967–986, http://dx.doi.org/10.1175/1520-0426(1996)013<0967:PCOAHS>2.0.CO;2.

Arnott, W.P., Hamasha, K., Moosmüller, H., Sheridan, P.J., Ogren, J. A., 2005. Towards aerosol light-absorption measurements with a

7-wavelength aethalometer: evaluation with a photoacoustic instrument and 3-wavelength nephelometer. Aerosol Sci. Technol. 39, 17—29, http://dx.doi.org/10.1080/027868290901972.

Anderson, T.L., Ogren, J.A., 1998. Determining aerosol radiative properties using the TSI 3563 integrating nephelometer. Aerosol Sci. Technol. 29, 57—69.

Chen, Y.-C., Hamre, B., Frette, Ø., Blindheim, S., Stebel, K., Sobolewski, P., Toledano, C., Stamnes, J.J., 2013. Aerosol optical properties in Northern Norway and Svalbard. Atmos. Meas. Tech. Discuss. 6, 10761—10795, http://dx.doi.org/10.5194/amtd-6-10761-2013.

Damoah, R., Spichtinger, N., Forster, C., James, P., Mattis, I., Wandinger, U., Beirle, S., Wagner, T., Stohl, A., 2004. Around the world in 17 days — hemispheric-scale transport of forest fire smoke from Russia in May 2003. Atmos. Chem. Phys. 4 (5), 1311—1321, http://dx.doi.org/10.5194/acp-4-1311-2004.

Draxler, R.R., Hess, G.D., 1998. An overview of the HYSPLIT_4 modelling system for trajectories. Aust. Meteorol. Mag. 47 (4), 295—308.

Hansen, A.D., Rosen, H., Novakov, T., 1984. The aethalometer—an instrument for the real-time measurement of optical absorption by aerosol particles. Sci. Total Environ. 36, 191—196, http://dx.doi.org/10.1016/0048-9697(84)90265-1.

Hämeri, K., Koivisto, A., Järvelä, M., Lyyranen, J., Auvinen, A., Jokiniemi, J., 2010. Optical Diameter of Mobility Classified Aerosol. American Association for Aerosol Research. Oregon Convention Center, Portland, OR, USA.

Jarraud, M., 2008. Guide to Meteorological Instruments and Methods of Observation (WMO-No. 8). World Meteorological Organisation, Geneva, Switzerland, 681 pp.

Lisok, J., Markowicz, K.M., Ritter, C., Makuch, P., Petelski, T., Chilinski, M., Kaminski, J.W., Becagli, S., Traversi, R., Udisti, R., Rozwadowska, A., Jefimow, M., Markuszewski, P., Neuber, R., Pakszys, P., Stachlewskaa, I.S., Struzewska, J., Zielinski, T., 2016. 2014 iAREA campaign on aerosol in Spitsbergen — Part 1: Study of physical and chemical properties. Atmos. Environ. 140, 150—166, http://dx.doi.org/10.1016/j.atmosenv.2016.05.051.

McFarquhar, G.M., Ghan, S., Verlinde, J., Korolev, A., Strapp, J.W., Schmid, B., Tomlinson, J.M., Wolde, M., Brooks, S.D., Cziczo, D., Dubey, M.K., Fan, J., Flynn, C., Gultepe, I., Hubbe, J., Gilles, M. K., Laskin, A., Lawson, P., Leaitch, W.R., Liu, P., Xiaohong, L., Lubin, D., Mazzoleni, C., MacDonald, A.M., Moffet, R.C., Morrison, H., Ovchinnikov, M., Shupe, M.D., Turner, D.D., Xie, S., Zelenyuk, A., Bae, K., Freer, M., Glen, A., 2011. Indirect and semi-direct aerosol campaign: the impact of Arctic aerosols on clouds. B. Am. Meteorol. Soc. 92 (2), 183—201.

Myhre Lund, C., Toledano, C., Myhre, G., Stebel, K., Yttri, K.E., Aaltonen, V., Johnsrud, M., Frioud, M., Cachorro, V., de Frutos, A., Lihavainen, H., Campbell, J.R., Chaikovsky, A.P., Shiobara, M., Welton, E.J., Tørseth, K., 2007. Regional aerosol optical properties and radiative impact of the extreme smoke event in the European Arctic in spring 2006. Atmos. Chem. Phys. 7 (22), 5899—5915, http://dx.doi.org/10.5194/acp-7-5899-2007.

O'Dowd, C., Monahan, C., Dall'Osto, M., 2010. On the occurrence of open ocean particle production and growth events. Geophys. Res. Lett. 37 (19), L19805, http://dx.doi.org/10.1029/2010GL044679.

Petelski, T., 2005. Coarse aerosol concentration over the North Polar Waters of the Atlantic. Aerosol Sci. Technol. 39 (8), 695—700, http://dx.doi.org/10.1080/02786820500182362.

Petelski, T., Markuszewski, P., Makuch, P., Jankowski, A., Rozwadowska, A., 2014. Studies of vertical coarse aerosol fluxes in the boundary layer over the Baltic Sea. Oceanologia 56 (4), 697—710, http://dx.doi.org/10.5697/oc.56-4.697.

Quinn, P.K., Shaw, G., Andrews, E., Dutton, E.G., Ruoho-Airola, T., Gong, S.L., 2007. Arctic haze: current trends and knowledge gaps. Tellus B 59 (1), 99—114.

Ritter, C., Neuber, R., Schulz, A., Markowicz, K.M., Stachlewska, I.S., Lisok, J., Makuch, P., Pakszys, P., Markuszewski, P., Rozwadowska, A., Petelski, T., Zielinski, T., Becagli, S., Traversi, R., Udisti, R., Gausa, M., 2016. 2014 iAREA campaign on aerosol in Spitsbergen — Part 2: Optical properties from Raman-lidar and in-situ observations at Ny-Ålesund. Atmos. Environ. 141, 1—19, http://dx.doi.org/10.1016/j.atmosenv.2016.05.053.

Rolph, G.D., 2016. Real-time Environmental Applications and Display sYstem (READY). NOAA Air Resources Laboratory, Silver Spring, MD Website (http://ready.arl.noaa.gov).

Rozwadowska, A., Sobolewski, P., 2010. Variability in aerosol optical properties at Hornsund, Spitsbergen. Oceanologia 52 (4), 599—620, http://dx.doi.org/10.5697/oc.52-4.599.

Rozwadowska, A., Zieliński, T., Petelski, T., Sobolewski, P., 2010. Cluster analysis of the impact of air back-trajectories on aerosol optical properties at Hornsund, Spitsbergen. Atmos. Chem. Phys. 10 (3), 87—893, http://dx.doi.org/10.5194/acp-10-877-2010.

Savelyev, I.B., Anguelova, M.D., Frick, G.M., Dowgiallo, D.J., Hwang, P.A., Caffrey, P.F., Bobak, J.P., 2014. On direct passive microwave remote sensing of sea spray aerosol production. Atmos. Chem. Phys. 14 (21), 11611—11631, http://dx.doi.org/10.5194/acp-14-11611-2014.

Schmid, O., Artaxo, P., Arnott, W.P., Chand, D., Gatti, L.V., Frank, G. P., Hoffer, A., Schnaiter, M., Andreae, M.O., 2006. Spectral light absorption by ambient aerosols influenced by biomass burning in the Amazon Basin. I: Comparison and field calibration of absorption measurement techniques. Atmos. Chem. Phys. 6 (11), 3443—3462, http://dx.doi.org/10.5194/acp-6-3443-2006.

Sharma, S., Andrews, E., Barrie, L.A., Ogren, J.A., Lavoue, D., 2006. Variations and sources of the equivalent black carbon in the high Arctic revealed by long-term observations at Alert and Barrow: 1989—2003. J. Geophys. Res. Atmos. 111 (D14), http://dx.doi.org/10.1029/2005JD006581.

Shaw, G.E., 1995. The Arctic haze phenomenon. B. Am. Meteorol. Soc. 76 (12), 2403—2413, http://dx.doi.org/10.1175/1520-0477(1995)076<2403:TAHP>2.0.CO;2.

Smirnov, A., Holben, B.N., Eck, T.F., Dubovik, O., Slutsker, I., 2003. Effect of wind speed on columnar aerosol optical properties at Midway Island. J. Geophys. Res. 108 (D24), 4802, http://dx.doi.org/10.1029/2003JD003879.

Stein, A.F., Draxler, R.R., Rolph, G.D., Stunder, B.J.B., Cohen, M.D., Ngan, F., 2015. NOAA's HYSPLIT atmospheric transport and dispersion modeling system. B. Am. Meteorol. Soc. 96, 2059—2077, http://dx.doi.org/10.1175/BAMS-D-14-00110.1.

Stock, M., Ritter, C., Aaltonen, V., Aas, W., Handorff, D., Herber, A., Treffeisen, R., Dethloff, K., 2014. Where does the optically detectable aerosol in the European Arctic come from? Tellus B 66, http://dx.doi.org/10.3402/tellusb.v66.21450.

Stohl, A., Andrews, E., Burkhart, J.F., Forster, C., Herber, A., Hoch, S.W., Kowal, D., Lunder, C., Mefford, T., Ogren, J.A., Sharma, S., Spichtinger, N., Stebel, K., Stone, R., Ström, J., Tørseth, K., Wehrli, C., Yttri, K.E., 2006. Pan-Arctic enhancements of light absorbing aerosol concentrations due to North American boreal forest fires during summer 2004. J. Geophys. Res. Atmos. 111 (D22), http://dx.doi.org/10.1029/2006JD007216.

Stone, R.S., Herber, A., Vitale, V., Mazzola, M., Lupi, A., Schnell, R. C., Dutton, E.G., Liu, P.S.K., Li, S.-M., Dethloff, K., Lampert, A., Ritter, C., Stock, M., Neuber, R., Maturilli, M., 2010. A three-dimensional characterization of Arctic aerosols from airborne Sun photometer observations: PAM-ARCMIP. J. Geophys. Res. Atmos. 115 (D13), http://dx.doi.org/10.1029/2009JD013605.

Svendsen, H., Beszczynska-Møller, A., Hagen, J.O., Lefauconnier, B., Tverberg, V., Gerland, S., Børre Ørbøk, J., Bischof, K., Papucci, C., Zajaczkowski, M., Azzolini, R., Bruland, O., Wiencke, C., Winther, J.-G., Dallmann, W., 2002. The physical environment of Kongsfjorden—Krossfjorden, an Arctic fjord system in Svalbard. Polar Res. 21 (1), 133—166, http://dx.doi.org/10.1111/j.1751-8369.2002.tb00072.x.

Tomasi, C., Kokhanovsky, A.A., Lupi, A., Ritter, C., Smirnov, A., O'Neill, N., Robert, T., Stone, S., Holben, B.N., Nyeki, S., Wehrli,

C., Stohl, A., Mazzola, M., Lanconelli, C., Vitale, V., Stebel, K., Aaltonen, V., de Leeuw, G., Rodriguez, E., Herber, A.B., Radionov, V.F., Zielinski, T., Petelski, T., Sakerin, S.M., Kabanov, D.M., Xue, Y., Mei, L., Istomina, L., Wagener, R., McArthur, B., Sobolewski, P. S., Kivi, R., Courcoux, Y., Larouche, P., Broccardo, S., Piketh, S. J., 2015. Aerosol remote sensing in polar regions. Earth-Sci. Rev. 140, 108—157.

Treffeisen, R., Tunved, P., Ström, J., Herber, A., Bareiss, J., Helbig, A., Stone, R.S., Hoyningen-Huene, W., Krejci, R., Stohl, A., Neuber, R., 2007. Arctic smoke—aerosol characteristics during a record smoke event in the European Arctic and its radiative impact. Atmos. Chem. Phys. 7 (11), 3035—3053, http://dx.doi.org/10.5194/acp-7-3035-2007.

Tunved, P., Ström, J., Krejci, R., 2013. Arctic aerosol life cycle: linking aerosol size distributions observed between 2000 and 2010 with air mass transport and precipitation at Zeppelin station. Ny-Ålesund. Svalbard., 2013. Atmos. Chem. Phys. 13 (7), 3643—3660, http://dx.doi.org/10.5194/acp-13-3643-2013.

Vaishya, A., Jennings, S.G., O'Dowd, C., 2012. Wind-driven influences on aerosol light scattering in north-east Atlantic air. Geopys. Res. Lett. 39 (5), L05805, http://dx.doi.org/10.1029/2011GL050556.

Virkkula, A., Ahlquist, N.C., Covert, D.S., Arnott, W.P., Sheridan, P. J., Quinn, P.K., Coffman, D.J., 2005. Modification, calibration and a field test of an instrument for measuring light absorption by particles. Aerosol Sci. Technol. 39 (1), 68—83, http://dx.doi.org/10.1080/027868290901963.

Walczowski, W., 2013. Frontal structures in the West Spitsbergen Current margins. Ocean Sci. 9 (6), 957—975, http://dx.doi.org/10.5194/os-9-957-2013.

Zieliński, T., 2004. Studies of aerosol physical properties in coastal areas. Aerosol Sci. Technol. 38 (5), 513—524, http://dx.doi.org/10.1080/02786820490466738.